Directed and elliptic flow of charged particles in Cu + Cu collisions at $\sqrt{s_{NN}} = 22.4$ GeV

G. Agakishiev,[17] M. M. Aggarwal,[29] Z. Ahammed,[47] A. V. Alakhverdyants,[17] I. Alekseev,[15] J. Alford,[18] B. D. Anderson,[18] C. D. Anson,[27] D. Arkhipkin,[2] G. S. Averichev,[17] J. Balewski,[22] D. R. Beavis,[2] N. K. Behera,[13] R. Bellwied,[43] M. J. Betancourt,[22] R. R. Betts,[7] A. Bhasin,[16] A. K. Bhati,[29] H. Bichsel,[49] J. Bielcik,[9] J. Bielcikova,[10] L. C. Bland,[2] I. G. Bordyuzhin,[15] W. Borowski,[40] J. Bouchet,[18] E. Braidot,[26] A. V. Brandin,[25] A. Bridgeman,[1] S. G. Brovko,[4] E. Bruna,[52] S. Bueltmann,[28] I. Bunzarov,[17] T. P. Burton,[2] X. Z. Cai,[39] H. Caines,[52] M. Calderón de la Barca Sánchez,[4] D. Cebra,[4] R. Cendejas,[5] M. C. Cervantes,[41] P. Chaloupka,[10] S. Chattopadhyay,[47] H. F. Chen,[37] J. H. Chen,[39] J. Y. Chen,[51] L. Chen,[51] J. Cheng,[44] M. Cherney,[8] A. Chikanian,[52] K. E. Choi,[33] W. Christie,[2] P. Chung,[10] M. J. M. Codrington,[41] R. Corliss,[22] J. G. Cramer,[49] H. J. Crawford,[3] Cui,[37] A. Davila Leyva,[42] L. C. De Silva,[43] R. R. Debbe,[2] T. G. Dedovich,[17] J. Deng,[38] A. A. Derevschikov,[31] R. Derradi de Souza,[6] L. Didenko,[2] P. Djawotho,[41] S. M. Dogra,[16] X. Dong,[21] J. L. Drachenberg,[41] J. E. Draper,[4] C. M. Du,[20] J. C. Dunlop,[2] L. G. Efimov,[17] M. Elnimr,[50] J. Engelage,[3] G. Eppley,[35] M. Estienne,[40] L. Eun,[30] O. Evdokimov,[7] R. Fatemi,[19] J. Fedorisin,[17] R. G. Fersch,[19] P. Filip,[17] E. Finch,[52] V. Fine,[2] Y. Fisyak,[2] C. A. Gagliardi,[41] D. R. Gangadharan,[27] F. Geurts,[35] P. Ghosh,[47] Y. N. Gorbunov,[8] A. Gordon,[2] O. G. Grebenyuk,[21] D. Grosnick,[46] A. Gupta,[16] S. Gupta,[16] W. Guryn,[2] B. Haag,[4] O. Hajkova,[9] A. Hamed,[41] L.-X. Han,[39] J. W. Harris,[52] J. P. Hays-Wehle,[22] M. Heinz,[52] S. Heppelmann,[30] A. Hirsch,[32] E. Hjort,[21] G. W. Hoffmann,[42] D. J. Hofman,[7] B. Huang,[37] H. Z. Huang,[5] T. J. Humanic,[27] L. Huo,[41] G. Igo,[5] P. Jacobs,[21] W. W. Jacobs,[14] C. Jena,[12] F. Jin,[39] J. Joseph,[18] E. G. Judd,[3] S. Kabana,[40] K. Kang,[44] J. Kapitan,[10] K. Kauder,[7] H. W. Ke,[51] D. Keane,[18] A. Kechechyan,[17] D. Kettler,[49] D. P. Kikola,[32] J. Kiryluk,[21] A. Kisiel,[48] V. Kizka,[17] S. R. Klein,[21] A. G. Knospe,[52] D. D. Koetke,[46] T. Kollegger,[11] J. Konzer,[32] I. Koralt,[28] L. Koroleva,[15] W. Korsch,[19] L. Kotchenda,[25] V. Kouchpil,[10] P. Kravtsov,[25] K. Krueger,[1] M. Krus,[9] L. Kumar,[18] M. A. C. Lamont,[2] J. M. Landgraf,[2] S. LaPointe,[50] J. Lauret,[2] A. Lebedev,[2] R. Lednicky,[17] J. H. Lee,[2] W. Leight,[22] M. J. LeVine,[2] C. Li,[37] L. Li,[42] N. Li,[51] W. Li,[39] X. Li,[32] X. Li,[38] Y. Li,[44] Z. M. Li,[51] L. M. Lima,[36] M. A. Lisa,[27] F. Liu,[51] H. Liu,[4] J. Liu,[35] T. Ljubicic,[2] W. J. Llope,[32] R. S. Longacre,[2] Y. Lu,[37] E. V. Lukashov,[25] X. Luo,[37] G. L. Ma,[39] Y. G. Ma,[39] D. P. Mahapatra,[12] R. Majka,[52] O. I. Mall,[4] R. Manweiler,[46] S. Margetis,[18] C. Markert,[42] H. Masui,[21] H. S. Matis,[21] D. McDonald,[35] T. S. McShane,[8] A. Meschanin,[31] R. Milner,[22] N. G. Minaev,[31] S. Mioduszewski,[41] M. K. Mitrovski,[2] Y. Mohammed,[41] B. Mohanty,[47] M. M. Mondal,[47] B. Morozov,[15] D. A. Morozov,[31] M. G. Munhoz,[36] M. K. Mustafa,[32] M. Naglis,[21] B. K. Nandi,[13] T. K. Nayak,[47] L. V. Nogach,[31] S. B. Nurushev,[31] G. Odyniec,[21] A. Ogawa,[2] K. Oh,[33] A. Ohlson,[52] V. Okorokov,[25] E. W. Oldag,[42] R. A. N. Oliveira,[36] D. Olson,[21] M. Pachr,[9] B. S. Page,[14] S. K. Pal,[47] Y. Pandit,[18] Y. Panebratsev,[17] T. Pawlak,[48] H. Pei,[7] T. Peitzmann,[26] C. Perkins,[3] W. Peryt,[48] P. Pile,[2] M. Planinic,[53] M. A. Ploskon,[21] J. Pluta,[48] D. Plyku,[28] N. Poljak,[53] J. Porter,[21] A. M. Poskanzer,[21] B. V. K. S. Potukuchi,[16] C. B. Powell,[21] D. Prindle,[49] C. Pruneau,[50] N. K. Pruthi,[29] P. R. Pujahari,[13] J. Putschke,[52] H. Qiu,[20] R. Raniwala,[34] S. Raniwala,[34] R. L. Ray,[42] R. Redwine,[22] R. Reed,[4] H. G. Ritter,[21] J. B. Roberts,[35] O. V. Rogachevskiy,[17] J. L. Romero,[4] L. Ruan,[2] J. Rusnak,[10] N. R. Sahoo,[47] I. Sakrejda,[21] S. Salur,[4] J. Sandweiss,[52] E. Sangaline,[4] A. Sarkar,[13] J. Schambach,[42] R. P. Scharenberg,[32] J. Schaub,[46] A. M. Schmah,[21] N. Schmitz,[23] T. R. Schuster,[11] J. Seele,[22] J. Seger,[8] I. Selyuzhenkov,[14] P. Seyboth,[23] N. Shah,[5] E. Shahaliev,[17] M. Shao,[37] M. Sharma,[50] S. S. Shi,[51] Q. Y. Shou,[39] E. P. Sichtermann,[21] F. Simon,[23] R. N. Singaraju,[47] M. J. Skoby,[32] N. Smirnov,[52] D. Solanki,[34] P. Sorensen,[2] U. G. deSouza,[36] H. M. Spinka,[1] B. Srivastava,[32] T. D. S. Stanislaus,[46] S. G. Steadman,[22] J. R. Stevens,[14] R. Stock,[11] M. Strikhanov,[25] B. Stringfellow,[32] A. A. P. Suaide,[36] M. C. Suarez,[7] N. L. Subba,[18] M. Sumbera,[10] X. M. Sun,[21] Y. Sun,[37] Z. Sun,[20] B. Surrow,[22] D. N. Svirida,[15] T. J. M. Symons,[21] A. Szanto de Toledo,[36] J. Takahashi,[6] A. H. Tang,[2] Z. Tang,[37] L. H. Tarini,[50] T. Tarnowsky,[24] D. Thein,[42] J. H. Thomas,[21] J. Tian,[39] A. R. Timmins,[43] D. Tlusty,[10] M. Tokarev,[17] S. Trentalange,[5] R. E. Tribble,[41] P. Tribedy,[47] B. A. Trzeciak,[48] O. D. Tsai,[5] T. Ullrich,[2] D. G. Underwood,[1] G. Van Buren,[2] G. van Nieuwenhuizen,[22] J. A. Vanfossen Jr.,[18] R. Varma,[13] G. M. S. Vasconcelos,[6] A. N. Vasiliev,[31] F. Videbæk,[2] Y. P. Viyogi,[47] S. Vokal,[17] S. A. Voloshin,[50] M. Wada,[42] M. Walker,[22] F. Wang,[32] G. Wang,[5] H. Wang,[24] J. S. Wang,[20] Q. Wang,[32] X. L. Wang,[37] Y. Wang,[44] G. Webb,[19] J. C. Webb,[2] G. D. Westfall,[24] C. Whitten Jr.,[5,*] H. Wieman,[21] S. W. Wissink,[14] R. Witt,[45] W. Witzke,[19] Y. F. Wu,[51] Z. Xiao,[44] W. Xie,[32] H. Xu,[20] N. Xu,[21] Q. H. Xu,[38] W. Xu,[5] Y. Xu,[37] Z. Xu,[2] L. Xue,[39] Y. Yang,[20] Y. Yang,[51] P. Yepes,[35] K. Yip,[2] I.-K. Yoo,[33] M. Zawisza,[48] H. Zbroszczyk,[48] W. Zhan,[20] J. B. Zhang,[51] S. Zhang,[39] W. M. Zhang,[18] X. P. Zhang,[44] Y. Zhang,[21] Z. P. Zhang,[37] F. Zhao,[5] J. Zhao,[39] C. Zhong,[39] X. Zhu,[44] Y. H. Zhu,[39] and Y. Zoulkarneeva[17]

(STAR Collaboration)

[1]*Argonne National Laboratory, Argonne, Illinois 60439, USA*

[2]*Brookhaven National Laboratory, Upton, New York 11973, USA*

[3]*University of California, Berkeley, California 94720, USA*

[4]*University of California, Davis, California 95616, USA*

[5]*University of California, Los Angeles, California 90095, USA*

[6]*Universidade Estadual de Campinas, CEP 13083-970 Sao Paulo, Brazil*

[7]*University of Illinois at Chicago, Chicago, Illinois 60607, USA*

[8]*Creighton University, Omaha, Nebraska 68178, USA*

[9]*Czech Technical University in Prague, FNSPE, Prague, CZ-115 19, Czech Republic*

[10]*Nuclear Physics Institute AS CR, CZ-250 68 Řež/Prague, Czech Republic*

[11]*University of Frankfurt, D-60325 Frankfurt, Germany*

 ©2012 American Physical Society

[12]*Institute of Physics, Bhubaneswar 751005, India*
[13]*Indian Institute of Technology, Mumbai 400076, India*
[14]*Indiana University, Bloomington, Indiana 47408, USA*
[15]*Alikhanov Institute for Theoretical and Experimental Physics, Moscow 117218, Russia*
[16]*University of Jammu, Jammu 180001, India*
[17]*Joint Institute for Nuclear Research, Dubna 141 980, Russia*
[18]*Kent State University, Kent, Ohio 44242, USA*
[19]*University of Kentucky, Lexington, Kentucky 40506-0055, USA*
[20]*Institute of Modern Physics, Lanzhou 730000, China*
[21]*Lawrence Berkeley National Laboratory, Berkeley, California 94720, USA*
[22]*Massachusetts Institute of Technology, Cambridge, Massachusetts 02139-4307, USA*
[23]*Max-Planck-Institut für Physik, D-80805 Munich, Germany*
[24]*Michigan State University, East Lansing, Michigan 48824, USA*
[25]*Moscow Engineering Physics Institute, Moscow 115409, Russia*
[26]*NIKHEF and Utrecht University, 1098 XG Amsterdam, The Netherlands*
[27]*Ohio State University, Columbus, Ohio 43210, USA*
[28]*Old Dominion University, Norfolk, Virginia, 23529, USA*
[29]*Panjab University, Chandigarh 160014, India*
[30]*Pennsylvania State University, University Park, Pennsylvania 16802, USA*
[31]*Institute of High Energy Physics, Protvino 142281, Russia*
[32]*Purdue University, West Lafayette, Indiana 47907, USA*
[33]*Pusan National University, Pusan, Republic of Korea*
[34]*University of Rajasthan, Jaipur 302004, India*
[35]*Rice University, Houston, Texas 77251, USA*
[36]*Universidade de Sao Paulo, CEP 05508-090 Sao Paulo, Brazil*
[37]*University of Science & Technology of China, Hefei 230026, China*
[38]*Shandong University, Jinan, Shandong 250100, China*
[39]*Shanghai Institute of Applied Physics, Shanghai 201800, China*
[40]*SUBATECH, F-44307 Nantes, France*
[41]*Texas A&M University, College Station, Texas 77843, USA*
[42]*University of Texas, Austin, Texas 78712, USA*
[43]*University of Houston, Houston, Texas 77204, USA*
[44]*Tsinghua University, Beijing 100084, China*
[45]*United States Naval Academy, Annapolis, Maryland 21402, USA*
[46]*Valparaiso University, Valparaiso, Indiana 46383, USA*
[47]*Variable Energy Cyclotron Centre, Kolkata 700064, India*
[48]*Warsaw University of Technology, PL-00-661 Warsaw, Poland*
[49]*University of Washington, Seattle, Washington 98195, USA*
[50]*Wayne State University, Detroit, Michigan 48201, USA*
[51]*Institute of Particle Physics, CCNU (HZNU), Wuhan 430079, China*
[52]*Yale University, New Haven, Connecticut 06520, USA*
[53]*University of Zagreb, Zagreb HR-10002, Croatia*

(Received 26 September 2011; revised manuscript received 7 December 2011; published 3 January 2012)

This paper reports results for directed flow v_1 and elliptic flow v_2 of charged particles in Cu + Cu collisions at $\sqrt{s_{NN}} = 22.4$ GeV at the Relativistic Heavy Ion Collider. The measurements are for the 0–60% most central collisions, using charged particles observed in the STAR detector. Our measurements extend to 22.4-GeV Cu + Cu collisions the prior observation that v_1 is independent of the system size at 62.4 and 200 GeV and also extend the scaling of v_1 with η/y_{beam} to this system. The measured $v_2(p_T)$ in Cu + Cu collisions is similar for $\sqrt{s_{NN}}$ throughout the range 22.4 to 200 GeV. We also report a comparison with results from transport model (ultrarelativistic quantum molecular dynamics and multiphase transport model) calculations. The model results do not agree quantitatively with the measured $v_1(\eta)$, $v_2(p_T)$, and $v_2(\eta)$.

DOI: 10.1103/PhysRevC.85.014901 PACS number(s): 25.75.Ld, 25.75.Dw

I. INTRODUCTION

The study of collective flow in relativistic nuclear collisions has potential to offer insights into the equation of state of

*Deceased.

the produced matter [1,2]. Anisotropic flow is conveniently characterized by the Fourier coefficients [3]

$$v_n = \langle \cos n(\phi - \Psi_R) \rangle, \quad (1)$$

where the angle brackets indicate an average over all the particles used, ϕ denotes the azimuthal angle of the outgoing particles, Ψ_R is the orientation of the reaction plane, and n denotes the harmonic. The reaction plane is defined by the beam axis and the vector connecting the centers of the two colliding nuclei. The estimated reaction plane is called the event plane, and its orientation is denoted above by Ψ_R. The procedure used in the present study to estimate this angle is explained in Sec. II C.

Directed flow, v_1, is the first harmonic coefficient of the Fourier expansion of the final-state momentum-space azimuthal anisotropy, and it reflects the collective sideward motion of the particles in the final state. Both hydrodynamic and nuclear transport models [4,5] indicate that directed flow is a promising observable for investigating a possible phase transition, especially in the region of relatively low beam energy under investigation in the present paper [6,7]. In particular, the shape of v_1 as a function of rapidity, y, in the midrapidity region is of interest because it has been argued that it offers sensitivity to crucial details of the expansion of the participant matter during the early stages of the collision. The models indicate that the evolving shape and orientation of the participant zone and its surface play a role in determining the azimuthal anisotropy measured among these particles in the final state.

It has been known for a long time that in the general vicinity of beam rapidity, the directed flow is dominated by a "bounce-off" effect, whereby particles are preferentially emitted within the reaction plane and are collectively deflected toward the side that corresponds to being repelled from the participant zone [8,9]. At RHIC energies, where the rapidity gap between beams is large (e.g., more than ten units at $\sqrt{s_{NN}} = 200$ GeV), the midrapidity region cannot be treated in terms of a monotonic interpolation between the rapidity regions on either side. Over a region of $\sqrt{s_{NN}}$ spanning ~20 to 200 GeV, it is inferred that the slope $dv_1/d\eta$ (where η is pseudorapidity) exhibits the algebraic sign associated with bounce-off near beam rapidities, but then $v_1(\eta)$ crosses zero at points well away from midrapidity, and the slope $dv_1/d\eta$ near midrapidity has the opposite sign [10,11].

The above phenomenon of $dv_1/d\eta$ or dv_1/dy having opposite sign near midrapidity had been predicted by hydrodynamic and nuclear transport models [12–15] and variations on this theme had been given names like "antiflow" or "third flow component" or "wiggle." It has been argued that this is a possible signature of a phase transition between hadronic matter and quark gluon plasma, especially if it is observed for identified baryons [15]. However, it is also possible to explain the qualitative features of the sign reversal in dv_1/dy in a purely hadronic picture by assuming strong but incomplete baryon stopping, together with strong space-momentum correlations caused by transverse radial expansion [14].

Elliptic flow, v_2, is the second harmonic coefficient of the Fourier expansion. The initial-state spatial eccentricity of the participant zone drives the process whereby the interactions produce an anisotropic distribution of momenta relative to the reaction plane. The elliptic anisotropy saturates quite early in the collision evolution, although a little later than when directed flow saturates [8,9]. Elliptic flow can provide information about the pressure gradients in a hydrodynamic description and about the effective degrees of freedom, the extent of thermalization, and the equation of state of the matter created at early times. Studying the dependence of elliptic flow on system size, number of constituent quarks, and transverse momentum or transverse mass are crucial to the understanding of the properties of the produced matter [1].

We find that directed flow violates the "entropy-driven" multiplicity scaling which dominates all other soft observables. STAR has reported an intriguing new universal scaling of the phenomenon with collision centrality [11]. Unlike the ratio of the elliptic flow parameter v_2 to the system initial eccentricity (ϵ), which scales with the particle density in the transverse plane, $v_1(\eta)$ at a given centrality is found to be independent of the system size and varies only with the incident energy. The different scalings for v_2/ϵ and v_1 might arise from the way in which they are developed: to produce v_2, many momentum exchanges among particles must occur, while to produce v_1, an important feature of the collision process is that different rapidity losses need to occur for particles at different distances from the center of the participant zone. This later quantity is related to incident energy. A recent $(3 + 1)$-dimensional hydrodynamic calculation has successfully reproduced various aspects of the measured directed flow for Au + Au and Cu + Cu at 200 GeV [16]. It is of interest to see if these features are followed at lower beam energies, as investigated in the current work.

We report here the first measurements of the directed and elliptic flow in Cu + Cu collisions from the STAR [17] experiment at the Relativistic Heavy Ion Collider (RHIC) at $\sqrt{s_{NN}} = 22.4$ GeV. The measurement of directed flow is presented as a function of pseudorapidity (η) and elliptic flow is presented as a function of pseudorapidity, transverse momentum (p_T), and centrality.

The paper is organized as follows: Section II briefly describes the detectors used and provides details of the analysis methods. In Sec. III, we present results on directed and elliptic flow (v_1 and v_2) and compare these with models. A summary is provided in Sec. IV.

II. EXPERIMENT AND ANALYSIS

A. STAR detector subsystems

The results presented here are based on data recorded by the STAR detector [17]. The time projection chamber (TPC) [18] is the primary tracking device at STAR. It is 4.2 m long and 4 m in diameter and its acceptance covers ± 1.0 units of pseudorapidity and has full azimuthal coverage. The charged-particle momenta are measured by reconstructing their trajectories through the TPC.

The charged-particle reconstruction at forward rapidities is provided by STAR's forward time projection chambers (FTPCs) [19]. The two FTPCs are located around the beam axis, one at each end of the STAR detector approximately 2.3 m from the nominal interaction region (IR), with

acceptance in the pseudorapidity range $2.5 \leqslant |\eta| \leqslant 4.0$ and with full azimuthal coverage.

The beam-beam counter (BBC) detector subsystem [20] consists of two detectors mounted around the beam pipe, each located outside the STAR magnet pole tip at opposite ends of the detector, approximately 375 cm from the center of the nominal IR. Each BBC detector consists of nearly circular scintillator tiles arranged in four concentric rings that provide full azimuthal coverage. The two inner rings have a pseudorapidity coverage of $3.3 < |\eta| < 5.0$ and are used to reconstruct the first-harmonic event plane (Ψ_1), for the directed flow analysis. The outer BBC tiles were not used.

B. Experimental data sets

The results presented in this paper are from Cu + Cu collisions at the nucleon-nucleon center-of-mass energy of $\sqrt{s_{NN}} = 22.4$ GeV with a minimum bias trigger based on BBC coincidences [20,21]. We present the results for the 0–60% most central events, for which the trigger efficiency was uniform. The primary collision vertex position along the beam direction (V_z) has a broad Gaussian distribution with a root mean square of 62 cm. Only events within 30 cm of the center of the detector are selected for this analysis. This value is chosen as a compromise between uniform detector performance within $|\eta| < 1.0$ and sufficient statistical significance of the measured observables. Event vertex is further required to be in the transverse direction within 2.0 cm from the center of the beam pipe in order to reject events which involve interactions with the beam pipe and to minimize beam-gas interactions. For directed flow analysis we further apply an event cut based on the maximum value of ADC signal from the BBC to avoid saturation of the BBC tiles. After these event cuts were applied the sample used for the directed flow analysis contained 350k events while the sample for the elliptic flow analysis consisted of 800k events.

Centrality classes in Cu + Cu collisions at $\sqrt{s_{NN}} = 22.4$ GeV are defined using the number of charged-particle tracks reconstructed in the TPC within pseudorapidity $|\eta| < 0.5$ and passing within 3 cm of interaction vertex. The uncorrected, i.e., not corrected for acceptance and reconstruction efficiency, multiplicity ($N_{\rm ch}$) distribution for events with a reconstructed primary vertex is shown in Fig. 1.

The directed and elliptic flow analyses were carried out on tracks that had transverse momenta $0.1 < p_T < 4.0$ GeV/c, passed within 3 cm of the primary vertex, had at least 15 space points in the main TPC acceptance ($|\eta| < 1.0$) or 5 space points in the case of tracks in the FTPC acceptance ($2.5 < |\eta| < 4.0$), and the ratio of the number of actual space points to the maximum possible number of space points for that tracks trajectory was greater than 0.52.

C. Flow methods

For any Fourier harmonic n, the event flow vector (Q_n) and the event-plane angle (Ψ_n) are defined by Ref. [3]

$$Q_n \cos(n\Psi_n) = Q_{nx} = \sum_i w_i \cos(n\phi_i), \tag{2}$$

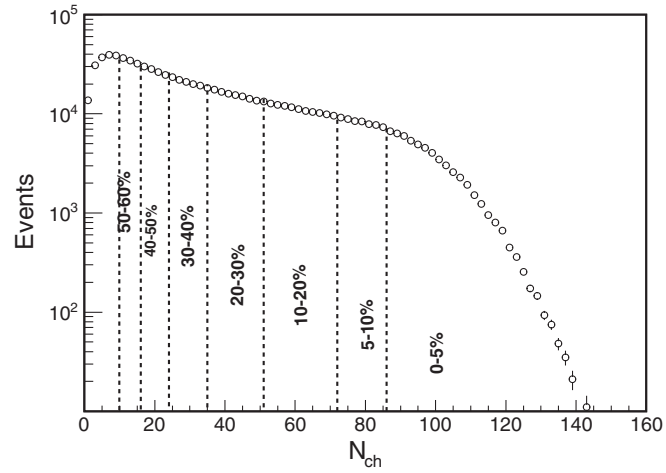

FIG. 1. Uncorrected multiplicity distribution with $|\eta| < 0.5$ in Cu + Cu collisions at $\sqrt{s_{NN}} = 22.4$ GeV. Events with $N_{\rm ch} > 10$ are selected for the present analysis.

$$Q_n \sin(n\Psi_n) = Q_{ny} = \sum_i w_i \sin(n\phi_i), \tag{3}$$

$$\Psi_n = \left(\tan^{-1}\frac{Q_{ny}}{Q_{nx}}\right)\Big/ n, \tag{4}$$

where sums extend over all particles i used in the event-plane calculation and ϕ_i and w_i are the laboratory azimuthal angle and the weight for the ith particle, respectively. In the case where we construct the event plane using tracks reconstructed from hits in the TPC or FTPC, weight for each particle is taken to be p_T in GeV/c up to 2.0 GeV/c and constant at 2.0 GeV/c for higher p_T [7]. In this case we denote the resulting flow harmonic as $v_n\{\text{TPC}\}$ or $v_n\{\text{FTPC}\}$. In those cases where the event plane is constructed using particle trajectories determined from hits in the BBC detectors, ϕ_i denotes the fixed azimuthal angle of the center of the ith BBC tile, and w_i is the energy deposition (the ADC signal, A_i) in the ith BBC tile and w_i is calculated from the ADC signals A_i, where

$$w_i = \frac{A_i}{\sum A_i}. \tag{5}$$

The corresponding flow harmonic is here denoted as $v_n\{\text{BBC}\}$. In all cases, the flow harmonic or coefficient is calculated by

$$v_n = \frac{\langle \cos n(\phi - \Psi_n)\rangle}{\langle \cos n(\Psi_n - \Psi_R)\rangle}. \tag{6}$$

where Ψ_R is the true reaction plane angle, Ψ_n is the event plane and the angle brackets here denote an average over all the particles in a specific bin in centrality. Tracks used for the calculation of v_n are excluded from the calculation of the event plane to remove self-correlation. The finite number of tracks limits the angular resolution of the reconstructed event plane. Consequently, the flow coefficient that is obtained with the reconstructed event plane, i.e., the numerator in Eq. (6), requires an event-plane resolution correction [3], which is the denominator in Eq. (6). The event-plane resolution is estimated from the correlation of the event planes of two subevents [3]. In the case of elliptic flow analysis, three

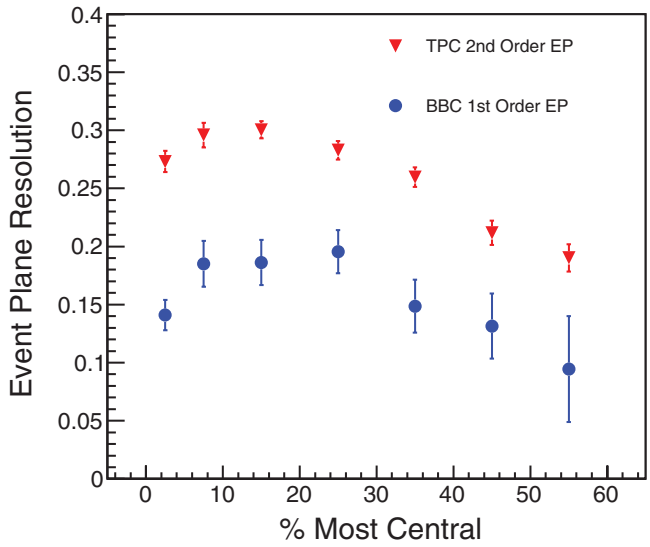

FIG. 2. (Color online) The event-plane resolution measured using the TPC (second order) and using the BBC (first order) are shown as a function of collision centrality for Cu + Cu collisions at $\sqrt{s_{NN}} = 22.4$ GeV. Errors are statistical only.

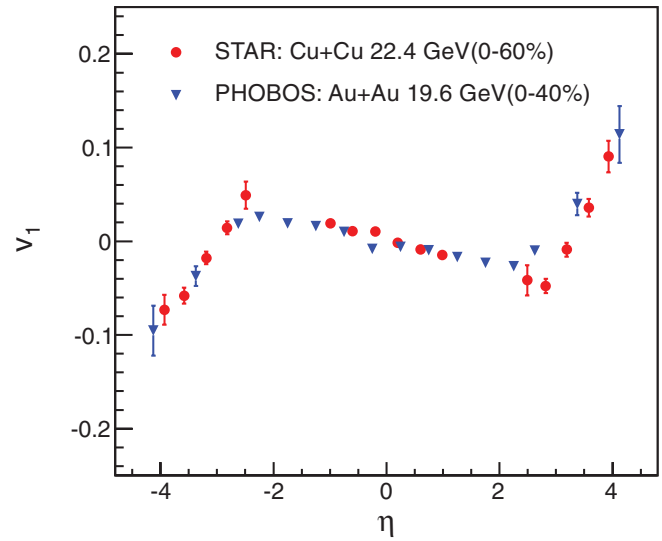

FIG. 3. (Color online) Charged hadron $v_1\{\text{BBC}\}$ vs. η for 0–60% centrality Cu + Cu collisions at $\sqrt{s_{NN}} = 22.4$ GeV. The errors shown are statistical. Systematic errors are discussed in Sec. III C. Results are compared to v_1 from 0–40% centrality Au + Au collisions at $\sqrt{s_{NN}} = 19.6$ GeV from the PHOBOS collaboration [10].

different ways have been tested for choosing the subevents: (i) Particles with pseudorapidity $-1.0 < \eta < -0.3$ are assigned to one subevent and particles with $0.3 < \eta < 1.0$ to the other subevent. The gap between the two pseudorapidity regions ensures that short-range correlations such as Bose-Einstein interference or Coulomb final-state interactions contribute negligibly to the observed correlations [22] and also may reduce possible jet effects, such as the minijet interpretation discussed in Ref. [23]. (ii) Particles are assigned randomly to two subevents. (3) Positive particles are assigned to one subevent and negative particles to the other. Figure 2 shows the event-plane resolution as a function of centrality, where the TPC second-order event-plane resolution was determined using the first (pseudorapidity) method described above. The average event-plane resolution for the $n = 2$ plane for $v_2\{\text{TPC}\}$ is 0.26 ± 0.01 for collisions with centrality 0–60%.

The BBC event plane obtained from one BBC detector is called a subevent plane. A combination of the sub-event-plane vectors for both BBC detectors provides the full event plane. In the $v_1\{\text{BBC}\}$ method, we used the BBC full event plane to obtain directed flow in the TPC pseudorapidity range ($|\eta| < 1.0$). A self-correlation arises if v_1 is obtained using particles from the same pseudorapidity region as used for the event-plane reconstruction. This problem can arise in the $v_1\{\text{BBC}\}$ analysis, because there is partial overlap in pseudorapidity coverage between the FTPC and the BBC. To avoid this, when v_1 was obtained in the FTPC coverage $-4.0 < \eta < -2.5$, the event plane was constructed using the BBC covering $3.3 < \eta < 5.0$ and, conversely, when using the FTPC coverage $2.5 < \eta < 4.0$ to determine v_1, the event plane was determined with the BBC covering $-5.0 < \eta < -3.3$. The first-order event-plane resolution as a function of centrality is shown in Fig. 2. The average event-plane resolution for the $n = 1$ plane for $v_1\{\text{BBC}\}$ is 0.16 ± 0.03 for collisions with centrality 0–60%.

III. RESULTS

A. Directed flow results

Figure 3 shows charged hadron $v_1\{\text{BBC}\}$ in Cu + Cu collisions for 0–60% centrality at $\sqrt{s_{NN}} = 22.4$ GeV as a function of η compared to that for 0–40% central Au + Au collisions at $\sqrt{s_{NN}} = 19.6$ GeV measured by the PHOBOS experiment [10]. The PHOBOS results are quite similar, notwithstanding the difference in system size and the fact that the centrality range and beam energy are not the same. At 200 and 62.4 GeV, we have previously reported that directed flow does not differ within errors for Au + Au and Cu + Cu [11]. We find that this behavior extends to lower energies. Directed flow provides information about the collision process that complements the more widely studied elliptic flow. Elliptic flow is developed after a number of momentum exchanges among particles, and the number of such exchanges depends on the dimensions of the participant system and on its density. Consequently, for a given collision centrality, elliptic flow varies with the mass of the colliding nuclei. In contrast, the observation that directed flow does not vary with the mass of the colliding nuclei is a reflection of the different mechanism that generates v_1: Here, the relevant feature is the rapidity shift undergone by particles that are initially located at different distances from the center of the participant volume [14]—a fundamental characteristic of the relativistic heavy-ion interaction process.

In Fig. 4 we compare our measurements to the results of the a multiphase transport (AMPT) [24] and ultrarelativistic quantum molecular dynamics (UrQMD) [25] models. Around midrapidity, the models predict a substantially smaller slope of $v_1(\eta)$ than that observed in the data, whereas at forward rapidities, the models differ among themselves and bracket the data. The fact that the tested models do not reproduce the

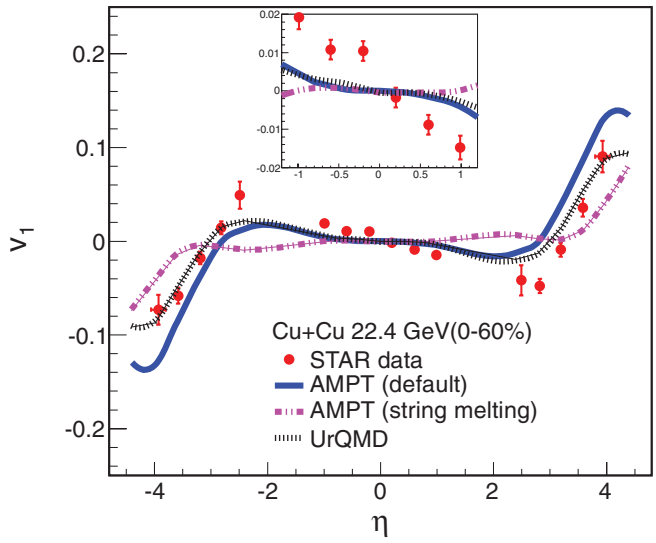

FIG. 4. (Color online) Comparison of the measured $v_1\{\text{BBC}\}$ as a function of η in 0–60% Cu + Cu collisions at $\sqrt{s_{NN}} = 22.4$ GeV with model predictions. The inset shows the central η region in more detail. The errors are statistical only.

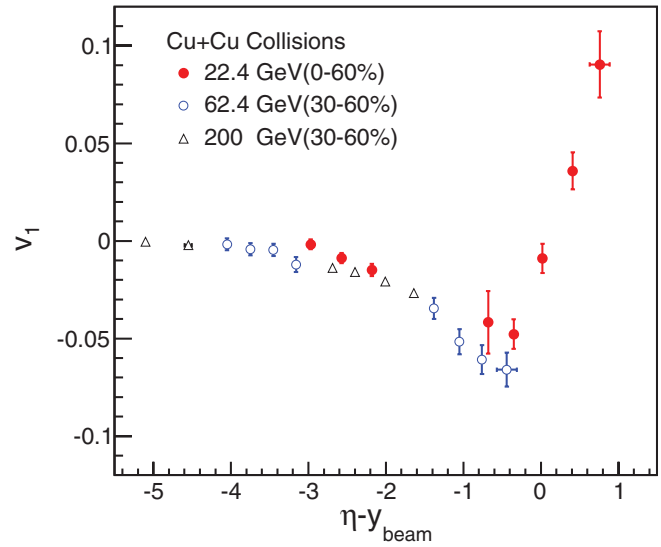

FIG. 6. (Color online) Charged hadron v_1 as a function of $\eta - y_{\text{beam}}$ values for the three beam energies 22.4, 62.4, and 200 GeV. The results for 62.4 and 200 GeV are for 30–60% centrality Cu + Cu collisions previously reported by STAR [11].

observed pattern of v_1 as a function of pseudorapidity implies the need for further evolution in the model descriptions.

Figure 5 shows charged hadron v_1 as a function of pseudorapidity scaled by the respective beam rapidity (y_{beam}) values for the three beam energies 22.4, 62.4, and 200 GeV in Cu + Cu collisions [11]. For Au + Au collisions over a range of $\sqrt{s_{NN}}$ spanning 19.6 to 200 GeV, it is an empirical observation that $v_1(\eta/y_{\text{beam}})$ lies close to a single common curve for all beam energies [10,11], and this type of scaling was first observed by NA49 at the SPS [26]. The new results

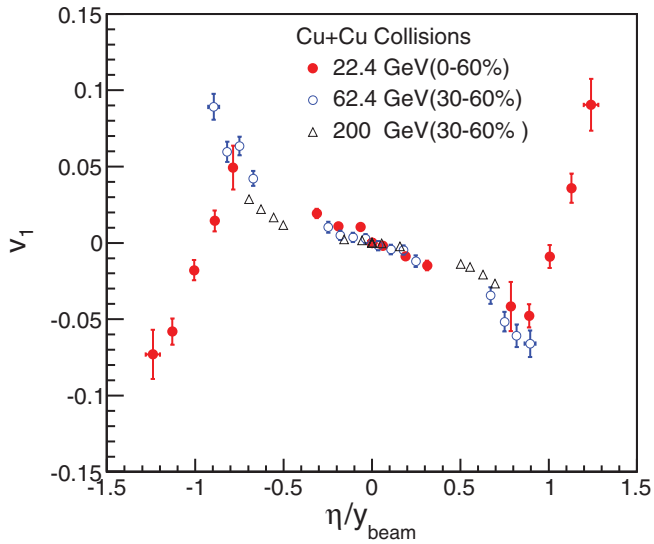

FIG. 5. (Color online) Charged hadron v_1 as a function of η, scaled by the respective y_{beam} for the three beam energies 22.4, 62.4, and 200 GeV. The results for 62.4 and 200 GeV are for 30–60% centrality Cu + Cu collisions previously reported by STAR [11]. For 22.4 GeV, the plotted results are for 0–60% centrality.

reported here for Cu + Cu at 22.4 GeV extend the range of applicability of this scaling behavior.

Figure 6 shows charged hadron v_1 as a function of $\eta - y_{\text{beam}}$, i.e., in the projectile frame for three beam energies 22.4, 62.4 and 200 GeV [11]. The data support the limiting fragmentation hypothesis [11] in the region $-2.6 < \eta - y_{\text{beam}} < 0$.

B. Elliptic flow results

Figure 7 shows $v_2(p_T)$ for charged hadrons from Cu + Cu collisions at $\sqrt{s_{NN}} = 22.4$ GeV measured with the subevent method with a pseudorapidity gap of 0.3 units. Also shown are the previously published STAR results for 200- and 62.4-GeV Cu + Cu [27] measured with the full TPC event-plane method $v_2\{\text{TPC}\}$ and full FTPC event-plane method $v_2\{\text{FTPC}\}$. The significant observed difference between $v_2\{\text{TPC}\}$ and $v_2\{\text{FTPC}\}$ at 200 GeV is discussed in detail in Ref. [27] and is attributed to the relatively large nonflow present in $v_2\{\text{TPC}\}$ for Cu + Cu at the top RHIC energy. We observe that the elliptic flow at 22.4 GeV is systematically lower than $v_2\{\text{TPC}\}$ at 200 GeV; however, it is similar to $v_2\{\text{FTPC}\}$ at 200 and 62.4 GeV, consistent with the earlier observation [28]. For comparison, we also show $v_2(p_T)$ from the UrQMD and AMPT models. The models do not agree with the data, but they do show an increase in v_2 with transverse-momentum similar to the data and plateau at much lower values of p_T. The small sample size in the present analysis precludes an extension of the measurements to identified particle v_2.

Figure 8 shows $v_2(\eta)$ for charged hadrons from Cu + Cu collisions at 0–60% centrality at $\sqrt{s_{NN}} = 22.4$ GeV. These STAR results are compared to published measurements from the PHOBOS Collaboration for 0–40% central collisions at $\sqrt{s_{NN}} = 22.4$ GeV [29]. The PHOBOS error bars include statistical and systematic errors, whereas the STAR data are plotted with statistical error bars only. Systematic errors are discussed in Sec. III C. The STAR results for $v_2(\eta)$ are

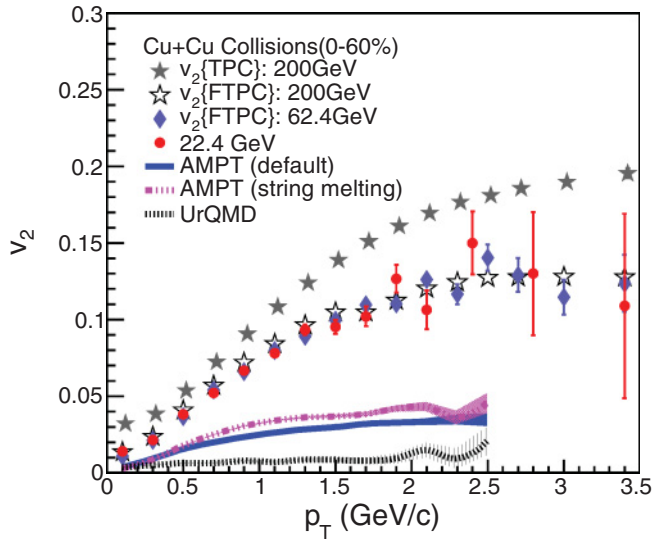

FIG. 7. (Color online) Elliptic flow versus p_T for charged hadrons from Cu + Cu collisions at 0–60% centrality at $\sqrt{s_{NN}} = 22.4$ GeV measured with the subevent method with a pseudorapidity gap of 0.3 units compared with previously published STAR results for 20- and 62.4-GeV Cu + Cu [27] measured with full TPC event-plane method $v_2\{\text{TPC}\}$ and full FTPC event-plane method $v_2\{\text{FTPC}\}$. The error bars are statistical. Results are also compared to $v_2(p_T)$ model calculations.

consistent within errors with the PHOBOS data. We also compare with corresponding predictions from the AMPT and UrQMD models. These models underpredict the data at midrapidity but do show a trend that is similar to the data for $|\eta| > 2.0$.

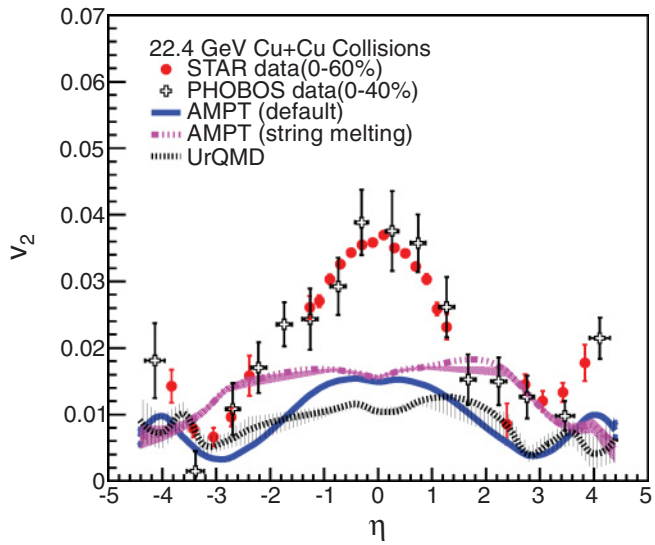

FIG. 8. (Color online) Elliptic flow $v_2(\eta)$ for charged hadrons from Cu + Cu collisions at 0–60% centrality at $\sqrt{s_{NN}} = 22.4$ GeV. The present STAR results are compared to the measurement from the PHOBOS [29] collaboration for Cu + Cu at 22.4 GeV. The PHOBOS results include statistical and systematic errors, whereas the STAR results are plotted with statistical uncertainties only, and systematic errors are discussed in Sec. III C.Results are also compared to $v_2(\eta)$ calculations from the indicated models.

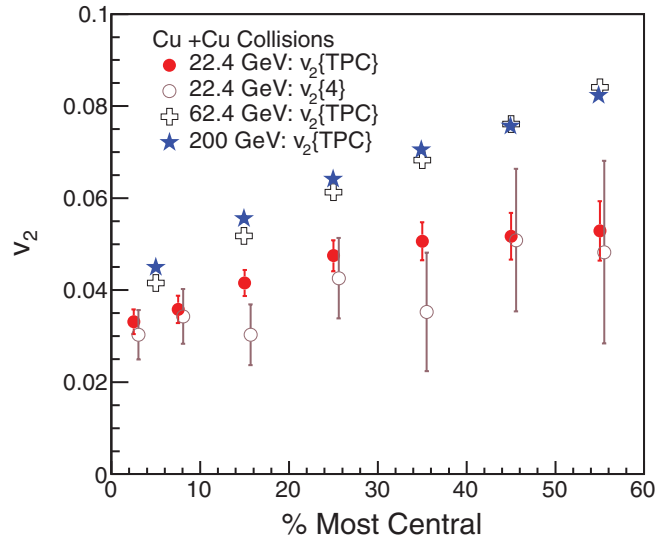

FIG. 9. (Color online) Elliptic flow $v_2\{\text{TPC}\}$ and $v_2\{4\}$ as a function of centrality for charged hadrons from Cu + Cu collisions at 0–60% centrality at $\sqrt{s_{NN}} = 22.4$ GeV compared with previously published results from the STAR collaboration at 200 and 62.4 GeV.

Figure 9 presents $v_2\{\text{TPC}\}$ for $0.1 < p_T < 2.0$ GeV/c and $|\eta| < 1.0$, as a function of centrality for charged hadrons from Cu + Cu collisions at 0–60% centrality at $\sqrt{s_{NN}} = 22.4$ GeV, plotted along with previously published results from the STAR collaboration at 200 and 62.4 GeV [27]. The present $v_2\{\text{TPC}\}$ result was obtained using η subevents [22] with a gap of 0.3 units in pseudorapidity while the published results are based on the full TPC. Also shown in Fig. 9 is a four-particle cumulant [30] analysis $v_2\{4\}$. This analysis method helps reduce some types of systematic error (see below) but generally requires more statistics than a method like $v_2\{\text{TPC}\}$. The statistical errors on our $v_2\{4\}$ measurements are small enough to be useful in the case of the more central collisions. The results from this $v_2\{4\}$ analysis agree, within statistical errors, with the $v_2\{\text{TPC}\}$ results, although there are hints of $v_2\{4\}$ being systematically lower than $v_2\{\text{TPC}\}$ for the more central data points. The beam energy dependence of the p_T-integrated v_2 mainly comes from the energy dependence of the mean p_T and the difference between the event-plane reconstruction with and without a pseudorapidity gap.

C. Systematic uncertainties

Any analysis of collective flow needs to consider the possible systematic uncertainty arising from nonflow [3], which refers to azimuthal correlations not related to the reaction-plane orientation. Nonflow can arise from resonances, jets, strings, quantum statistics effects, final-state interactions (particularly Coulomb effects), and momentum conservation. Different methods used to measure anisotropic flow are affected by nonflow in different ways and are used in this analysis to guide our estimates of the systematic uncertainty. In general, nonflow arising from jets can be expected to be less troublesome at lower beam energies. Moreover, as described earlier, the relatively large pseudorapidity gap between the STAR TPC and the BBCs is helpful in suppressing nonflow.

When the event plane is determined from a detector that is not symmetric around $\eta = 0$, we need to account for correlations in the measured directed flow due to momentum conservation [31]. The desired BBC η symmetry is present for our v_1 analysis in the η region of the central TPC but is a source of possible concern for the FTPC η region. The overlap in η acceptance between the BBC and FTPC is only partial, and, therefore, it is feasible to compare $v_1\{\text{BBC}\}_{\text{full}}$ (where both east and west BBCs are used) with $v_1\{\text{BBC}\}_{\text{sub}}$, using either the east or west BBC event plane for $2.5 < |\eta| < 3.3$. We find that the difference is less than 10%, and an extrapolated average correction has been applied to $v_1\{\text{BBC}\}$ for $|\eta| > 3.3$.

The measured v_1 must be antisymmetric about midpseudorapidity within statistical errors. Any larger difference is due to systematic errors. Previous detailed studies point to the maximum forward-backward difference as a viable estimate of the overall systematic uncertainty when the pseudorapidity gap is large [22]. We conclude that the overall systematic uncertainty in our determination of v_1 is approximately 15% in the FTPC region and about 10% in the central TPC region.

In our analysis of elliptic flow, v_2, unlike for directed flow, v_1, we do not have the advantage of a wide η gap to help ensure that nonflow background effects are minimized. To study possible systematic effects associated with short range nonflow correlations, a four-particle cumulant [30] analysis $v_2\{4\}$ as a function of centrality has been investigated and is plotted in Fig. 9. This method suppresses nonflow correlations involving fewer than four particles. The statistical errors on our $v_2\{4\}$ measurements are small enough to be useful for the most central collisions but grow to a few tens of percentages at the other end of our studied centrality range. The $v_2\{\text{TPC}\}$ and $v_2\{4\}$ measurements agree within statistical errors, although the observed systematic difference, which might arise from nonflow effects, amounts to about 9% for the 0–10% most central collisions.

In the elliptic flow measurement, we have used the η subevent method with a gap of 0.3 units in pseudorapidity (η). As noted in Sec. II C, such a gap suppresses short-range correlations such as Bose-Einstein interference and Coulomb final-state interactions. To estimate the nonflow contributions to our estimate of $v_2\{\text{TPC}\}$ due to these short-range correlations, we have studied variations in the resulting $v_2\{\text{TPC}\}$ induced by varying the event vertex selection along the beam direction, by varying the DCA cut value, and by varying the size of the pseudorapidity gap between the subevents in the η subevent method. Tests of this type suggest that the systematic error on v_2 is on the order of 10%. However, based on an alternative approach [23] to fitting and interpreting the measured data at 62.4 and 200 GeV, it is argued that the systematic uncertainty could be larger.

IV. SUMMARY

In this study of Cu + Cu collisions at $\sqrt{s_{NN}} = 22.4$ GeV, we present results at midrapidity and at forward rapidity for directed flow v_1 and elliptic flow v_2 as a function of pseudorapidity, and for elliptic flow v_2 as a function of transverse momentum at midrapidity for charged hadrons. For our directed flow measurement, nonflow correlations are expected to be strongly suppressed by the large pseudorapidity gap between the detector used for event-plane determination (BBC) and the main tracking detector (TPC) used in our directed flow measurement. Our estimate of the systematic error on the directed flow $v_1\{\text{BBC}\}$ is not more than 10 to 15% for the TPC and FTPC regions, respectively. Our findings for Cu + Cu and Au + Au at 22.4 GeV extend observations previously made at 62.4 and 200 GeV that directed flow is independent of system size in this energy region. Our findings also demonstrate that $v_1(\eta/y_{\text{beam}})$ remains independent of beam energy down to 22.4 GeV, a scaling behavior that has already been established at 62.4 and 200 GeV. We find that directed flow violates the "entropy-driven" multiplicity scaling which dominates all other soft observables. An important feature associated with generation of v_1 in the of the collision process is that different rapidity losses need to occur for particles at different distances from the center of the participant zone, which is beam-energy dependent. Measurements of the elliptic flow for 22.4 GeV Cu + Cu collisions are also presented. We compare p_T-integrated v_2 with measurements at higher energies. The p_T dependence of the measured v_2 at 22.4 GeV is similar to that at 62.4 and 200 GeV. UrQMD and AMPT models (the latter both with and without string melting) do not agree with the present measurements for both first (v_1) and second (v_2) coefficients.

ACKNOWLEDGMENTS

We thank the RHIC Operations Group and RCF at BNL, the NERSC Center at LBNL and the Open Science Grid consortium for providing resources and support. This work was supported in part by the Offices of NP and HEP within the US DOE Office of Science; the US NSF; the Sloan Foundation; the DFG cluster of excellence "Origin and Structure of the Universe" of Germany; CNRS/ IN2P3, FAPESP CNPq of Brazil; Ministry of Education and Science of the Russian Federation, NNSFC, CAS, MoST, and MoE of China; GA and MSMT of the Czech Republic; FOM and NWO of the Netherlands; DAE, DST, and CSIR of India; Polish Ministry of Science and Higher Education; Korea Research Foundation; Ministry of Science, Education and Sports of the Republic of Croatia; and RosAtom of Russia.

[1] I. Arsene *et al.* (BRAHMS Collaboration), Nucl. Phys. A **757**, 1 (2005); B. B. Back *et al.* (PHOBOS Collaboration), *ibid.* **757**, 28 (2005); J. Adams *et al.* (STAR Collaboration), *ibid.* **757**, 102 (2005); K. Adcox *et al.* (PHENIX Collaboration), *ibid.* **757**, 184 (2005).

[2] J.-Y. Ollitrault, Phys. Rev. D **46**, 229 (1992).

[3] A. M. Poskanzer and S. A. Voloshin, Phys. Rev. C **58**, 1671 (1998).

[4] U. W. Heinz, in *Relativistic Heavy Ion Physics*, Landolt-Boernstein New Series, Vol. I/23, edited by R. Stock (Springer Verlag, New York, 2010).

[5] S. A. Bass *et al.*, Prog. Part. Nucl. Phys. **41**, 225 (1998).

[6] M. M. Aggarwal *et al.* (STAR Collaboration) arXiv:1007.2613 (unpublished).
[7] B. I. Abelev *et al.* (STAR Collaboration), Phys. Rev. C **81**, 024911 (2010).
[8] H. Sorge, Phys. Rev. Lett. **78**, 2309 (1997).
[9] N. Herrmann, J. P. Wessels, and T. Wienold, Annu. Rev. Nucl. Part. Sci. **49**, 581 (1999).
[10] B. B. Back *et al.* (PHOBOS Collaboration), Phys. Rev. Lett. **97**, 012301 (2006).
[11] B. I. Abelev *et al.* (STAR Collaboration), Phys. Rev. Lett. **101**, 252301 (2008).
[12] L. P. Csernai and D. Rohrich, Phys. Lett. B **458**, 454 (1999).
[13] J. Brachmann *et al.*, Phys. Rev. C **61**, 024909 (2000).
[14] R. J. M. Snellings, H. Sorge, S. A. Voloshin, F. Q. Wang, and N. Xu, Phys. Rev. Lett. **84**, 2803 (2000).
[15] H. Stöcker, Nucl. Phys. A **750**, 121 (2005).
[16] P. Bozek and I. Wyskiel, Phys. Rev. C **81**, 054902 (2010).
[17] K. H. Ackermann *et al.*, Nucl. Instrum. Methods A **499**, 624 (2003).
[18] M. Anderson *et al.*, Nucl. Instrum. Methods A **499**, 659 (2003).
[19] K. H. Ackermann *et al.*, Nucl. Instrum. Methods A **499**, 713 (2003).
[20] C. A. Whitten Jr. (STAR Collaboration), AIP Conf. Proc. **980**, 390 (2008).
[21] F. S. Bieser *et al.*, Nucl. Instrum. Methods A **499**, 766 (2003).
[22] J. Adams *et al.* (STAR Collaboration), Phys. Rev. C **72**, 014904 (2005).
[23] D. T. Kettler (STAR Collaboration), Proc. of Workshop on Critical Examination of RHIC Paradigms, Univ. of Texas, Austin, TX, April 2010, PoS **CERP2010**, 011 (2011); T. A. Trainor, J. Phys. G **37**, 085004 (2010).
[24] Z. W. Lin and C.-M. Ko, Phys. Rev. C **65**, 034904 (2002); L.-W. Chen and C.-M. Ko, J. Phys. G **31**, S49 (2005).
[25] S. A. Bass *et al.*, Prog. Part. Nucl. Phys. **41**, 225 (1998); M. Bleicher *et al.*, J. Phys. G **25**, 1859 (1999).
[26] C. Alt *et al.* (NA49 Collaboration), Phys. Rev. C **68**, 034903 (2003).
[27] B. I. Abelev *et al.* (STAR Collaboration), Phys. Rev. C **81**, 044902 (2010).
[28] B. I. Abelev *et al.* (the STAR Collaboration), Phys. Rev. C **75**, 054906 (2007).
[29] R. Nouicer (for the PHOBOS Collaboration), J. Phys. G **34**, S887 (2007).
[30] A. Bilandzic, R. Snellings, and S. A. Voloshin, Phys. Rev. C **83**, 044913 (2011).
[31] N. Borghini, P. M. Dinh, J. Y. Ollitrault, A. M. Poskanzer, and S. A. Voloshin, Phys. Rev. C **66**, 014901 (2002).